Available online at www.sciencedirect.com
ScienceDirect
Journal of the European Ceramic Society 30 (2010) 857–863
www.elsevier.com/locate/jeurceramsoc

Effect of mullite additions on the fracture mode of alumina

Olga Burgos-Montes, Rodrigo Moreno, Carmen Baudín *

Instituto de Cerámica y Vidrio (CSIC), C/Kelsen 5, E-28049 Madrid, Spain

Received 19 May 2009; received in revised form 7 October 2009; accepted 20 October 2009
Available online 22 November 2009

Abstract

This work analyses the effect of mullite additions on the fracture mode of alumina. Mullite is proposed as an alternative to SiC for the second phase particles because the thermal expansion mismatch between alumina and mullite is of the same sign and order as that between alumina and SiC. Three alumina–5 vol.% mullite composites formed by alumina matrices with similar average grain sizes in the micrometric range (≈1 μm) and second phase sub-micrometric (50–350 nm) and nanometric mullite (<50 nm) particles located at grain boundaries and triple points were prepared. The fracture mode of the alumina matrix changed from predominantly intergranular to predominantly transgranular. This change became more significant as the size of the sub-micrometric fraction of mullite particles decreased.

Keywords: Slip cast; Nanocomposites; Fracture; Al_2O_3; Mullite

1. Introduction

Since the initial work by Niihara[1] alumina/SiC nanocomposites have been widely studied. Significant room temperature strength improvements (20–50%) together with very slight or no toughness increases have been reported by different authors.[1–4] Now it is known that the observed strength increases are partially due to the refinement of the structure by the limiting of the alumina grain growth by Zener pinning of SiC particles. Also, Niihara[1] has reported creep improvement for the alumina/SiC nanocomposites and attributed it to dislocation pinning by the SiC particles. Nevertheless, as signalled by Ortiz-Merino and Todd,[4] the most remarkable and reproducible benefits offered by the alumina–SiC nanocomposites are in their tribological properties, where great improvements compared with pure alumina in the resistance to severe wear, and surface finish following grinding and polishing have been reported. There is currently no accepted general explanation for these effects.

There is a general agreement on the fact that even very small amounts (≈2–5 vol.%) of SiC nanoparticles originate a change of the fracture mode of the alumina matrix from predominantly intergranular to predominantly transgranular; thus, limiting the pull-out sizes under wear conditions.[4,5] The origin of the fracture mode change is not completely clear. It has been attributed to the compressive residual stresses developed at the alumina grain boundaries by intra-granular SiC particles due to thermal expansion mismatch between alumina and SiC. Such stresses would have a shielding effect more pronounced than the grain boundary opening effect eventually associated with the thermal expansion anisotropy of alumina.[6–9] For this explanation to be correct, particle location inside the alumina grains is essential. In this sense, Ferroni and Pezzotti[9] reported that transgranular crack propagation in alumina/SiC nanocomposites depended on the location of the SiC dispersoids within the matrix texture; the higher the fraction of dispersoids located inside the alumina grains, determined by quantitative fractography analysis, the more transgranular the fracture mode. On the contrary, data reported for a wide range of aluminas and nanocomposites with systematic variations in the main microstructural features (alumina and SiC sizes, SiC location, 2, 5 and 10 vol.%) indicated that intra-granular particles were not necessary to change the fracture mode of alumina[4,10,11] and that it may even be preferable for them to be on the grain boundaries for 2 vol.% SiC nanocomposites.[4,5] Therefore, the possibility that the primary explanation is a chemical in origin rather than being a mechanical effect has been raised.

Alumina–mullite nanocomposites with small mullite amounts have also been reported by Zhang et al.[12,13] to present increased strength and wear resistance as compared to that of monophase alumina. In these composites, that have slightly reduced toughness, the fracture mode of alumina experiences

* Corresponding author. Tel.: +34 917 355 840; fax: +34 917 355 843.
E-mail address: cbaudin@icv.csic.es (C. Baudín).

0955-2219/$ – see front matter © 2009 Elsevier Ltd. All rights reserved.
doi:10.1016/j.jeurceramsoc.2009.10.013

the same transition from intergranular to transgranular as that observed in the alumina–SiC composites. As discussed by the authors, the change in the bulk mechanical properties of the materials could not explain the reduction of the area fraction of pull-out on the worn surfaces; conversely, it could be originated by the change in the fracture mode, as in alumina–SiC. The authors claimed the change of fracture mode to be originated by the residual stresses present in the alumina matrix due to the thermal expansion mismatch between alumina and the intra-granular mullite particles, which should be of the same sign as that between alumina and SiC. The studied materials were fabricated from alumina–SiC green bodies, by sintering in oxidizing atmosphere; the finer and larger mullite particles were described to be located inside the grains and at the grain boundaries, respectively.

In this work, the fracture behaviour of alumina + 5 vol.% mullite composites prepared by different routes leading to different mullite particle sizes has been studied. The fracture behaviour has been compared to that of a monophase alumina material fabricated using the same alumina raw material and with similar density and grain size as the alumina matrices in the composites.

2. Experimental

Three different alumina + 5 vol.% of mullite materials and one reference monophase alumina were fabricated. In all cases, a commercial α-alumina (Condea HPA05, USA) with an average particle size of 0.4 μm and specific surface area of 9 m^2/g was used.

For the fabrication of the composites, three different kinds of green bodies were prepared. Two of them, A5M and A5MC, were prepared by mixing alumina and 5 vol.% of mullite powders to a relative ratio of 95/5 (v/v) whereas the other one, A5MRS, was made from a mixture of alumina and colloidal silica suspension (LEVASIL 200A/40%, Germany) containing 40 wt.% particles with an average size of 15 nm, specific surface area of 200 m^2/g and pH of 9. Colloidal silica was added in the concentration needed to obtain 5 vol.% mullite after sintering. A5M specimens were fabricated from the as received alumina powders and commercial mullite powders (Baikalox, Baikowski, France) which were attrition milled for 7 h up to reach an average particle size of 0.7 μm.[14] For the A5MC compacts a porous mullite powder (particle sizes ≈100 μm) synthesized by combustion process[15] was attrition milled for 5 h down to an average particle size of 3 μm.

Concentrated suspensions of alumina/mullite 95/5 (v/v) and alumina/silica 98.2/1.8 (v/v) were prepared in deionised water to total solid loadings of 50 vol.% (75 wt.%). The alumina, silica and mullite suspensions were independently prepared and then mixed in the adequate proportions to obtain the composite suspensions. In all cases 1.2 wt.% of an ammonium salt of a polyacrylic acid PAA (Duramax D3005, Rohm & Haas, PA, USA) was added as a polyelectrolyte to provide electrosteric stabilisation at moderate pH values. The composite suspensions were homogenised in alumina jar mill for 6 h. In all cases, the final pH of the obtained suspensions was 6–7 and it did not change significantly with time. The green compacts were obtained by slip casting on plaster of Paris moulds and treated at 1550 °C/2 h, using heating and cooling rates of 5 °C/min in an electrical box furnace (Termiber, Spain) to obtain the final materials A5M, A5MC and A5MRS. The presence of mullite in the reaction sintered specimens (A5MRS) was confirmed by X-ray diffraction, XRD, using an apparatus with a lynx eye (D8 Advance, Bruker, Germany). Diffractions corresponding to the 0 1 2 plane for alumina (ASTM 46-1212) and the 1 2 0 and 2 1 0 planes for mullite (ASTM01-079-1458) were recorded using a step of 0.05 and exposure time of 5 s.

Additional green compacts were fabricated from the as received alumina and the attrition milled mullite powders by isostatic pressing (200 MPa). Alumina was sintered at 1450 during 1 h to reach 99% of theoretical density. Mullite was sintered at 1630 °C during 4 h to reach 97% of theoretical density. Specimens for elastic properties and thermal expansion determinations were diamond cut and rectified from the sintered compacts. Plates (3 mm × 40 mm × 40 mm) were used for Young's modulus and Poisson's coefficient determinations from the resonance frequency of the plates tested by impact in flexure and shear, determined using a commercial apparatus (Grindosonic, Lemmens, Leuven, Belgium). Parallelepipedic (4 mm × 6 mm × 15 mm) specimens were tested in a linear voltage displacement transducer dilatometer (Adhamel Lomargy, Roissy en Brie, France) with a quartz rod for the determination of the average thermal expansion coefficients between room temperature and 1000 °C. Three samples were tested for each material.

Apparent densities were determined using the EN 1389:2003 standard and relative densities were calculated using 3.987 g/cm^3 (ASTM-46-1212) and 3.16 g/cm^3 (ASTM-15-776) for alumina and mullite, respectively.

Sintered composite and monophase alumina specimens were diamond polished (down to 3 μm) and indented using 100 N. Afterwards, they were thermally etched at 1400 °C/1 h with a heating rate of 5 °C/min. Fractured pieces were obtained by impact. The microstructure of the composite materials was determined in the polished and fractured samples by field emission scanning electron microscope (FE-SEM, Hitachi S-4700 type I, Japan). The alumina grain size distributions were determined from FE-SEM micrographs of polished random cut surfaces samples using an image processing and analysis program (Leica Qwin, Leica Microsystems Ltd, Cambridge, England) considering more than 300 grains for each material. The program calculates the diameters of the equivalent spheres from the measured areas of the grains. From these values, the true diameter of the particles was calculated using the Abercrombieĭs factor ($4/\pi^{1/2}$).[16] For mullite, diameters of the particles were directly evaluated in polished and fracture surfaces. The fracture mode of the alumina grains, in terms of number of grains presenting trans- or intergranular fracture was quantified on the indentation crack paths. FE-SEM micrographs at 10,000× were taken randomly and the fracture mode of the grains interacting with the cracks was established. At least 50 grains were considered for each material.

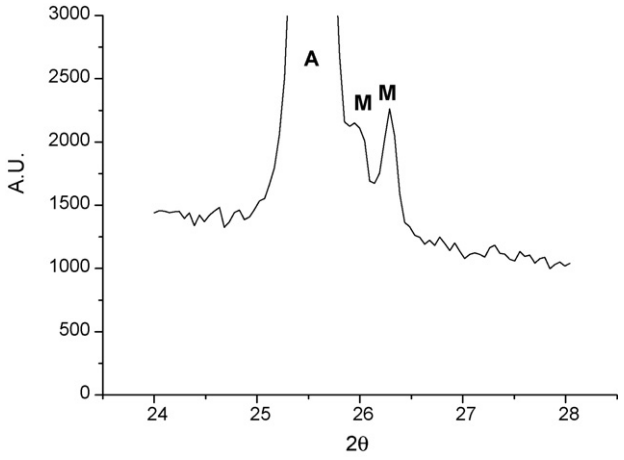

Fig. 1. X-ray diffraction patterns for the material A5MRS. The 0 1 2 peak for alumina (ASTM 46-1212) and the 1 2 0 and 2 1 0 peaks for mullite (ASTM01-079-1458) are signalled.

3. Results and discussion

Fig. 1 shows the characteristic XRD peaks of mullite (planes 1 2 0, $d = 3.4273$, and 2 1 0, $d = 3.3874$) for the reaction sintered material, A5MRS, demonstrating the presence of the crystalline mullite.

All composites were made of the same alumina powder (0.003 and 0.001 wt.% of Na_2O and Fe_2O_3, respectively) thus, any compositional difference would come from mullite. The main impurity related to mullite was Na_2O, coming from LEVASIL (0.2 wt.%) or from Baikowski mullite (0.18 wt.%). Calculations taking into account the composition of the materials give similar total amounts of Na_2O in the three materials (0.005 wt.% in the AMC and AMRS composites and 0.01 wt.% in the AM composite). Thus, the composite materials presented slightly higher amounts of Na_2O that the monophase alumina. Moreover, some residual silica might be present in the composites which, added to the impurities will lead to the formation of residual glass located at triple points and/or grain boundaries. If this were the case, the grain boundaries would be weakened as compared to those of the monophase alumina which is contrary to what was observed, as discussed below. Therefore, the effect of the small compositional differences on the fracture mode can be neglected.

Characteristic micrographs of polished surfaces of the reference alumina and the three composites showing indentation

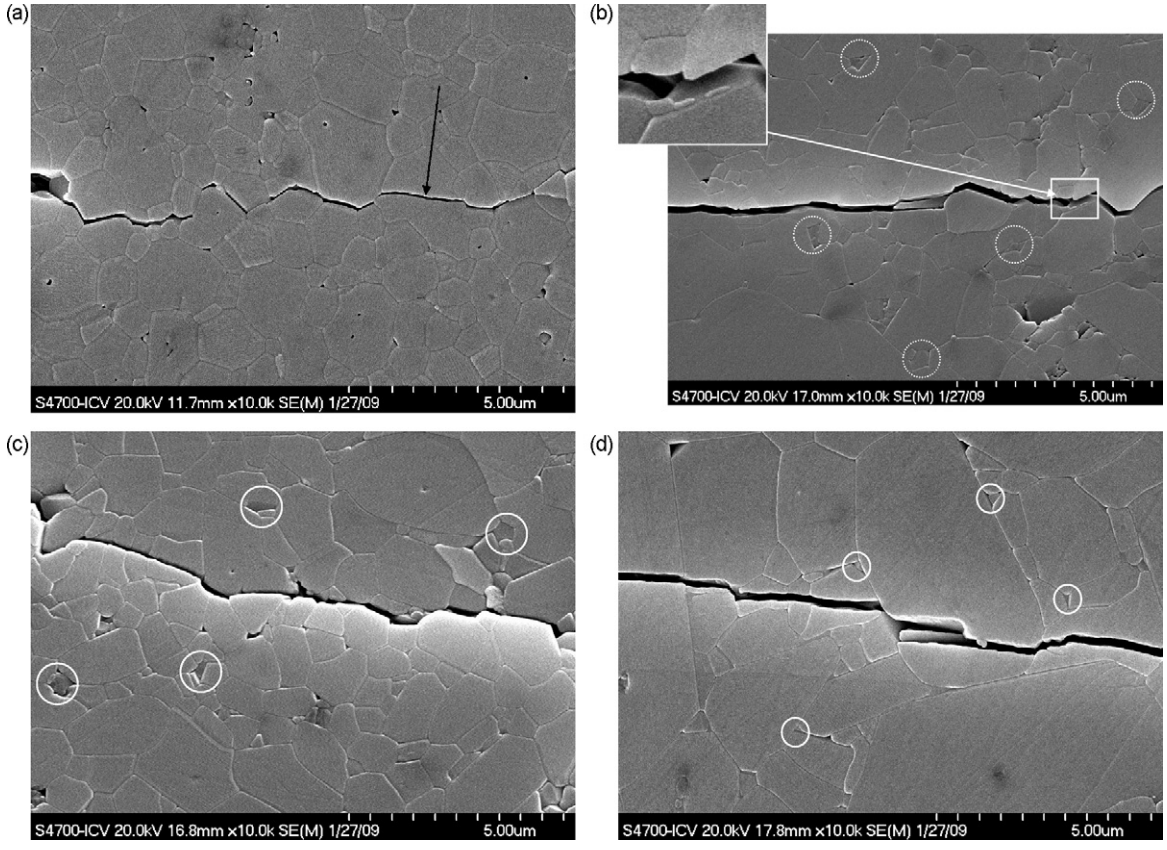

Fig. 2. FE-SEM of polished and thermally etched specimens showing characteristic microindentation cracks. (a) Monophase alumina specimen, A. Intergranular fracture is mostly observed. Only the largest grains are traversed by the crack (arrow). (b) Alumina + 5 vol.% composite from commercial mullite powders, A5M. Mixed trans-intergranular fracture is observed. Even sub-micrometric alumina grains present transgranular fracture (enlarged region). Small mullite grains (average diameter ≈300 nm) of darker gray are observed (some of them are encircled to highlight). (c) Alumina + 5 vol.% composite from mullite powders fabricated by combustion, A5MC. Mixed trans-intergranular fracture is observed. Small (average diameter ≈ 370 nm) mullite grains of darker gray are observed at alumina triple points and grain boundaries (some of them are encircled to highlight). (d) Reaction sintered alumina–5 vol.% mullite composite specimen, A5MRS. Transgranular fracture is mostly observed. Small (≈240 μm) mullite grains of darker gray are observed at alumina triple points and grain boundaries (some of them are encircled to highlight).

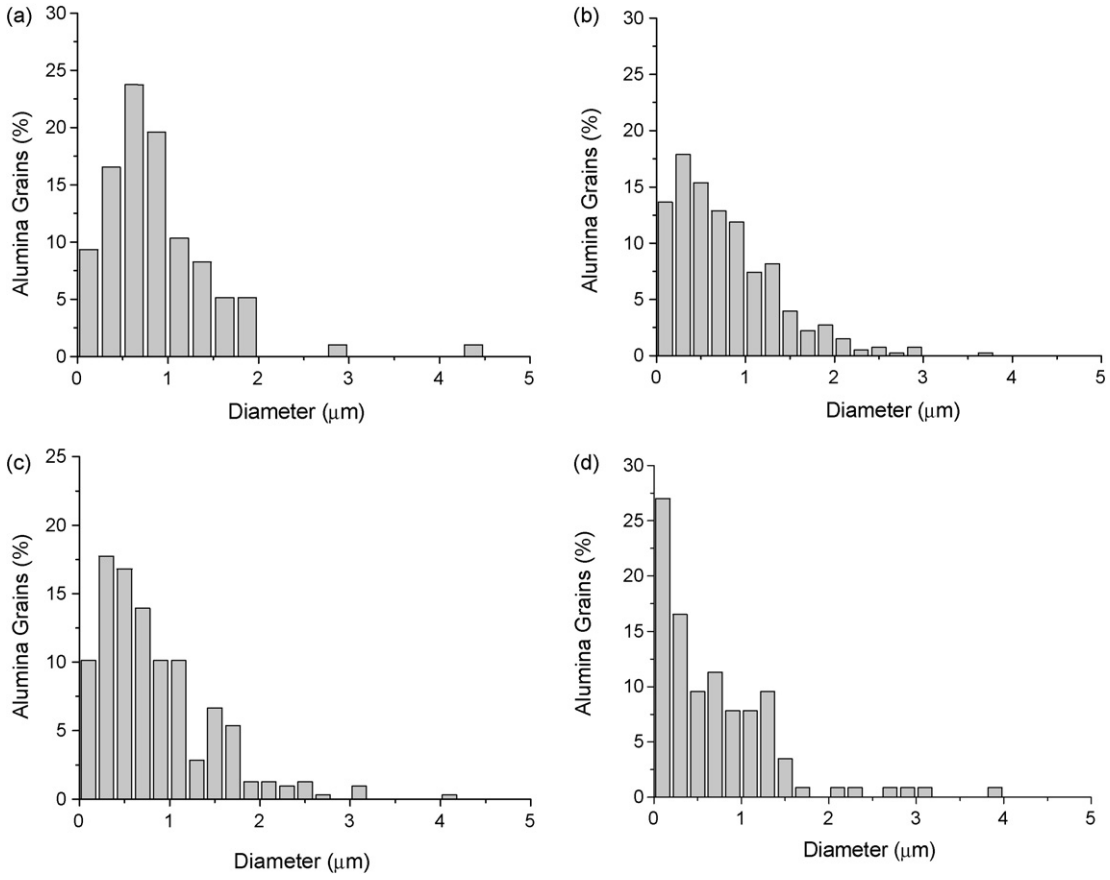

Fig. 3. Alumina grain size distributions. (a) Monophase alumina specimen, A. (b) Alumina + 5 vol.% composite from commercial mullite powders, A5M. (c) Alumina + 5 vol.% composite from mullite powders fabricated by combustion, A5MC. (d) Reaction sintered alumina–5 vol.% mullite composite specimen, A5MRS.

cracks are presented in Fig. 2. The corresponding alumina grain size distributions are plotted in Fig. 3. Fig. 4 shows characteristic fracture surfaces of the composites. Table 1 summarises the quantitative microstructural and fracture mode parameters.

Average alumina grain sizes were similar for all of the materials (Table 1) and most alumina grains in the four materials had sizes under 2.5 μm (Figs. 1 and 2; 2.1, 2.4, 3.8 and 4.3% of grains between 2.5 and 5 μm, for A, A5M, A5MC and A5MRS, respectively).

Since the four materials were dense (>96% of theoretical, Table 1) and presented similar grain sizes, the behavioural differences during fracture could be attributed to the presence of mullite secondary phase and its characteristics.

The fracture mode in the monophase alumina was mostly intergranular (Fig. 2a, Table 1) with only the largest grains being traversed by the crack, as is generally observed in high purity fine grained aluminas. This fracture mode changed significantly in the composites, as more than 64% of the alumina grains were traversed by the crack in the composites vs 21% in the monophase alumina (Figs. 2b–d, and 4, Table 1). In the A5MRS material there were observed some large grains abnormally grown (Fig. 2d) that were traversed by the crack. Nevertheless, the relative amount of large grains in this material as compared to alumina (4.3% vs 2.1% grains between 2.5 and 5 μm) cannot explain the amount of fracture mode change.

In the four composites, sub-micrometric (50–400 μm; average sizes ≈300, 370 and 240 nm, for materials A5M, A5MC and A5MRS, respectively) mullite grains were observed homogeneously dispersed at alumina triple points and grain boundaries in the polished surfaces (Fig. 2b–d). Additionally,

Table 1
Characteristics of the studied materials.

Material	Density (g/cm^3)	Relative density (% ρ_{th})	Fracture mode	Number of grains (%)	Average alumina grain size (sd) (μm)
			Intergranular	Transgranular	
A	3.90 ± 0.03	98 ± 1	79	21	1.0 (0.7)
A5M	3.84 ± 0.03	99 ± 1	30	70	0.9 (0.7)
A5MC	3.80 ± 0.03	96 ± 1	36	64	1.0 (0.7)
A5MRS	3.92 ± 0.03	99 ± 1	18	82	0.9 (1.0)

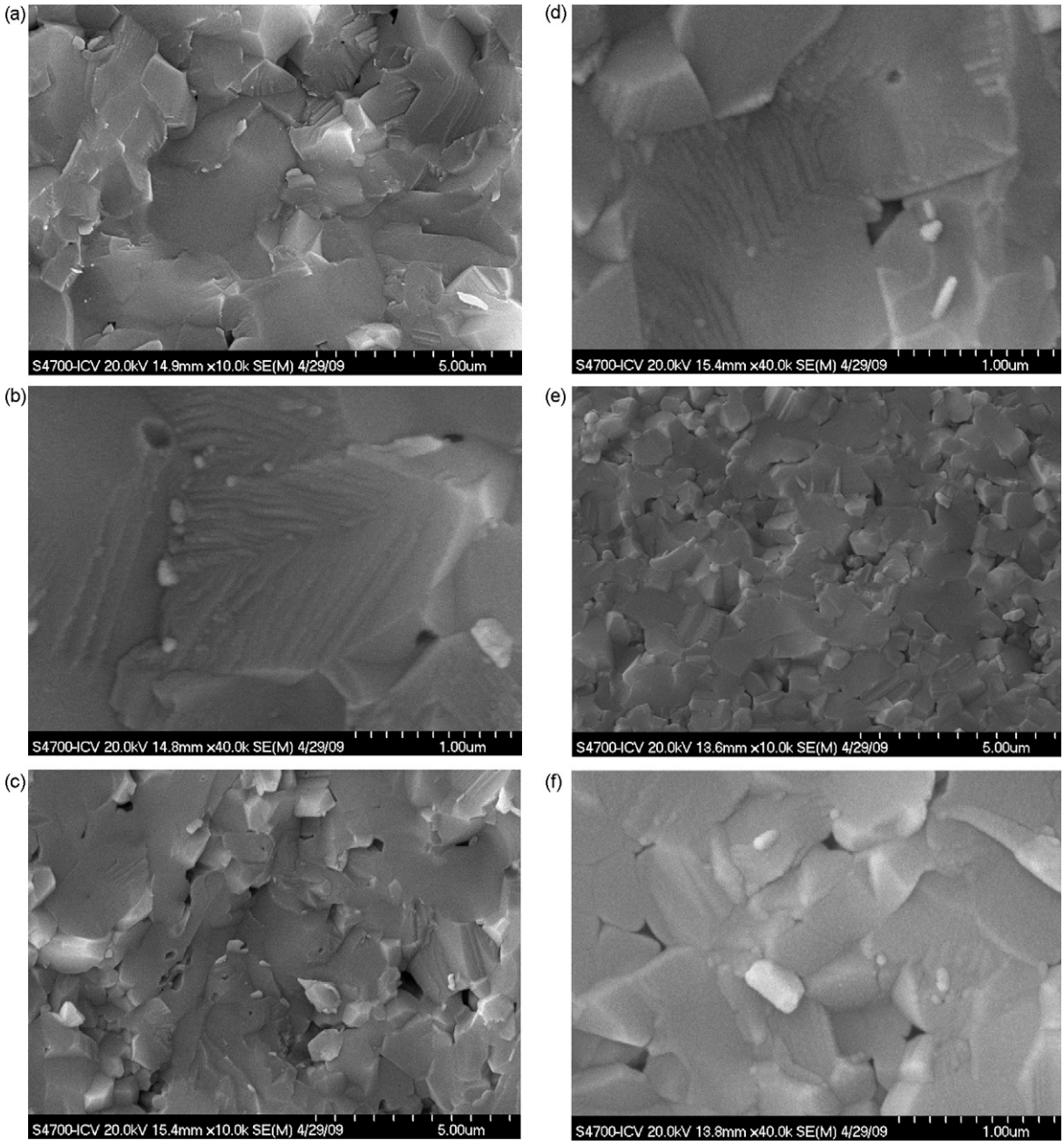

Fig. 4. Characteristic fracture surfaces of the studied alumina + 5 vol.% mullite composites. FE-SEM micrographs. Most alumina grains present transgranular fracture. Nanometric mullite grains (<50 nm) are revealed by the fracture (clearer colour) inside the alumina grains and at grain boundaries and triple points. (a, b) Alumina + 5 vol.% composite from commercial mullite powders, A5M. (c, d) Alumina + 5 vol.% composite from mullite powders fabricated by combustion, A5MC. (e, f) Alumina + 5 vol.% composite fabricated by reaction sintering of alumina and colloidal silica, A5MRS.

nanometric (<50 nm) mullite grains were revealed in the fracture surfaces (Fig. 4).

The material that presented the highest proportion of transgranular fracture, A5MRS, had the smallest average mullite grain size in FE-SEM micrographs and numerous nanometric particles were revealed in the fracture surfaces of this composite (Fig. 4e–f). Both materials fabricated from mixtures of alumina and mullite powders, A5M and A5MC, presented a lower proportion of transgranular fracture than the reaction sintered one, A5MRS, and the mullite particles were significantly larger. The composite fabricated from commercial powders, A5M, with higher transgranular fracture mode than A5MC (Table 1), had smaller mullite particle sizes in the polished surfaces ($\approx$ 300, 370 nm for A5M and A5MC) and, moreover, numerous nanometric grains were detected in the fracture surfaces (Fig. 4b).

As a summary, the three alumina–5 vol.% mullite composites presented homogeneous microstructures formed by alumina matrices with similar average grain sizes in the micrometric range ($\approx$1 μm) and second phase sub-micrometric (50–350 nm) and nanometric mullite (<50 nm) particles located at grain boundaries and triple points. The failure mode of the alumina matrix was changed from intergranular, for a monophase alumina material fabricated from the same alumina powder and similar grain sizes, into mixed trans-intergranular in the com-

posites. The extent of transgranular fracture mode increased for decreasing sizes of the mullite grains.

As discussed in the introduction, the change of fracture mode has been observed by different authors in alumina–SiC and alumina–mullite nanocomposites. Moreover, it has also been reported for a 10 vol.% SiC microcomposite with SiC sizes of about 3 μm[10] and for a 2 vol.% SiC microcomposite with SiC sizes of about 1 μm.[4] However, no quantitative evaluation of the extent of change as a function of the size of second phase particles has been reported.

As discussed above, the alumina matrix in alumina–mullite composites should develop residual stresses upon cooling of the same sign as those developed in alumina–SiC composites. The hydrostatic stress caused by the thermal mismatch in the alumina matrix is given by:

$$\sigma^A = K^*(T_0 - T)(\alpha_A - \alpha_M) \quad (1)$$

T_0 represents the temperature below which the stresses cannot be relaxed by plastic deformation, α_A and α_M are the thermal expansion coefficients of alumina and the second phase, respectively, and K^* is an effective elastic modulus which depends on the elastic constants and volume fractions, $f_{A,M}$, of the component phases as well as on the sample topology.[17] For second phase particles embedded in a continuous matrix.[18]

$$K^* = \frac{3nK_AK_Mf_M}{K_Mf_A + nK_Af_A + nK_Mf_M + K_Mf_M} \quad (2)$$

K is the bulk modulus ($K = (E/3 - 2\nu)$), where ν is the Poisson's coefficient.

The densities, the elastic properties and the thermal expansion coefficients of the monophase alumina and mullite materials used for the determination of the elastic and thermal expansion parameters together with those of a dense SiC reported by other authors[19] are summarised in Table 2. From the elastic data and the densities, the Young's modulus for 100% density materials, E_0, are calculated using the well known relationship:

$$E = E_0 \exp(-bP) \quad (3)$$

where E is the Young's modulus of a material with P porosity and $b = 3$ for alumina materials with spherical pores.

Assuming $T_0 = 1200\,^\circ$C for alumina materials, the calculated residual stresses at room temperature in the alumina matrix are, not only of the same sign but also of the same order for alumina–SiC (65 MPa) and alumina–mullite (73 MPa) composites. It is important to remark that these stresses are rather low and that they will decrease as the temperature of the material increases. For $T = 500\,^\circ$C, a flash temperature easily achieved during wear processes on ceramic specimens,[20] the residual stresses will be significantly reduced (≈40%). Thus, it is most probable for the observed change in the fracture mode of the alumina–mullite composites subjected to wear[10] not to be associated to residual stresses. Moreover, it has been observed that the fracture mode of alumina–SiC composites is also predominantly transgranular at high temperature.[21]

Apart from the development of residual stresses due to thermal expansion mismatch, the fracture mode of the matrix in a composite might change due to the modification of the grain boundary fracture energy, G_{gb}, by the second phase particles.[22] The fracture mode will be determined by the existing relationships between G_{gb}, the fracture energy of the interface between the second phase and the matrix particles G_i, and the transgranular fracture energy G_{cl}. When $G_i/G_{gb} > 1$, the particle strengthens the grain boundary whereas for $G_i/G_{gb} < 1$, the particle weakens the grain boundary. Moreover, the relationship between G_i and G_{cl} indicates when a change in crack propagation mode is likely. When $G_i/G_{cl} \geq 1$, an approaching intergranular crack would tend to become transgranular instead of proceeding by the tougher interface and when $G_i/G_{cl} < 1$ it would tend to propagate along the interface. Other factors influencing the failure mode will be residual stresses and the extra energy required for deflection.The relationships between G_i, G_{gb} and G_{cl}, are determined by the surface energies of the matrix, $\gamma_s{}^m$, and the particles, $\gamma_s{}^p$, the grain boundary energy, γ_{gb}, and the interfacial energy, γ_i:

$$\frac{G_i}{G_{cl}} = \frac{\gamma_s^m + \gamma_s^p - \gamma_i}{2\gamma_s^m} \quad (4)$$

$$\frac{G_i}{G_{gb}} = \frac{\gamma_s^m + \gamma_s^p - \gamma_i}{2\gamma_s^m - \gamma_{gb}} \quad (5)$$

As there are no reported values for the surface free energy of mullite, it is not possible to determine using Eqs. (4) and (5) whether the condition for approaching intergranular cracks to become transgranular instead of proceeding along the tougher interface are fulfilled. Nevertheless, some comments can be made about the effect of the mullite particles on the interfacial energy. Assuming that a particle on a grain boundary achieves thermodynamic equilibrium, grain boundary-interface dihedral angles can be used to correlate interfacial energy with grain boundary energy, as proposed by Jiao and co-workers.[23]

$$\frac{\gamma_l}{\gamma_{gb}} = \frac{1}{\cos\theta_1 + \sin\theta_1 \times \cos\theta_2/\sin\theta_2} = \frac{\sin\theta_2}{\sin(\theta_1 + \theta_2)} \quad (6)$$

Table 2
Materials properties used for calculations.

Material	Young's modulus (GPa) 100%TD	Experimental			
		Poisson's ratio	Average $CTE_{25-800\,^\circ C}$ ($\times 10^{-6}\,^\circ C^{-1}$)	Young's modulus (GPa)	%TD
Alumina	422	0.223 ± 0.004	8.4 ± 0.2	405 ± 5	98.8 ± 0.5
Silicon carbide[19]	431	0.16	5.0	415	98.7
Mullite	226	0.274 ± 0.006	4.1 ± 0.1	206 ± 3	97.1 ± 0.4

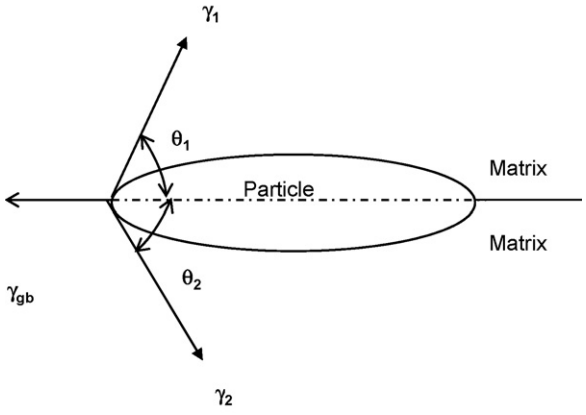

Fig. 5. Schematic of a particle on a grain boundary with the relevant parameters.

$$\frac{\gamma_2}{\gamma_{gb}} = \frac{1}{\cos\theta_2 + \sin\theta_2 \times \cos\theta_1/\sin\theta_1} = \frac{\sin\theta_1}{\sin(\theta_1+\theta_2)} \quad (7)$$

where $\theta = \theta_1 + \theta_2$ is the grain boundary-interface dihedral angle (Fig. 5).

Assuming symmetry ($\theta_1 = \theta_2 = \theta/2$; $\gamma_1 = \gamma_2 = \gamma_i$) and taking into account Eqs. (4) and (5), low dihedral angles ($\theta < 120^\circ$) correspond to $\gamma_i < \gamma_{gb}$; from Eqs. (6) and (7), low values of the interfacial energy lead to lower values of the interfacial fracture energy. High dihedral angles correspond to round particles, as in alumina–SiC composites whereas faceted particles such as most of the mullite particles observed in the materials studied here present low dihedral angles ($\leq 90^\circ$, Fig. 5). Thus, in principle, mullite additions would be adequate for grain boundary strengthening of the alumina matrix.

For materials with the same mullite amounts, grain boundary modifications will be more effective as mullite grain sizes decrease because the proportion of alumina–mullite grain boundaries will increase, as occurs in the series of materials studied here.

Data obtained in this work together with those previously reported for alumina–mullite composites fabricated by oxidation of alumina–SiC mixtures[12,13] indicate that this system has potential for thermodynamically stable ceramic composites with improved mechanical behaviour.

4. Conclusions

Dense materials of alumina–vol.% mullite have been prepared by slip casting mixtures of either alumina/silica followed by reaction sintering or alumina/mullite and conventional sintering. Low dihedral angles at the alumina/mullite interfaces suggest grain boundary strengthening of the alumina matrix. The incorporation of such small additions of sub-micrometric mullite changes the fracture mode of the alumina matrix from predominantly intergranular to predominantly transgranular. This change becomes more significant as the size of the coarsest fraction of mullite particle decreases.

Acknowledgement

This work has been supported by MICINN, MAT2006-13480 C02, Spain.

References

1. Niihara K. New design concept of structural ceramics–ceramic nanocomposites. *J Ceram Soc Jpn* 1991;**99**(10):974–82.
2. Zhao J, Stearns LC, Harmer MP, Chan HM, Miller GA. Mechanical behavior of alumina–silicon carbide "nanocomposites". *J Am Ceram Soc* 1993;**76**(2):505–10.
3. Sternitzke M. Review: structural ceramic nanocomposites. *J Eur Ceram Soc* 1997;**17**(9):1061–82.
4. Ortiz-Merino JL, Todd RI. Relationship between wear rate, surface pull-out and microstructure during abrasive wear of alumina and alumina/SiC nanocomposites. *Acta Mater* 2005;**53**:3345–57.
5. Winn AJ, Todd RI. Microstructural requirements for alumina–SiC nanocomposites. *British Ceram Trans* 1999;**98**(5):219–24.
6. Kovalev S, Ohji T, Yamauchi Y, Sakai M. Grain boundary strength in non-cubic ceramic polycrystals with misfitting intragranular inclusions (nanocomposites). *J Mater Sci* 2000;**35**:1405–12.
7. Pezzotti G, Müller WH. Strengthening mechanism in Al_2O_3/SiC nanocomposites. *Comput Mater Sci* 2001;**22**:155–68.
8. Levin I, Kaplan WD, Brandon DG. Effect of SiC submicrometric particle size and content on fracture toughness of alumina–SiC "nanocomposites". *J Am Ceram Soc* 1995;**78**(11):245–56.
9. Ferroni LP, Pezzotti G. Evidence for bulk residual stress strengthening in Al_2O_3/SiC nanocomposites. *J Am Ceram Soc* 2002;**85**(8):2033–8.
10. Limpichaipanit A, Todd RI. The relationship between microstructure, fracture and abrasive wear in Al_2O_3/SiC nanocomposites and microcomposites containing 5 and 10% SiC. *J Eur Ceram Soc* 2009;**29**:2841–8.
11. Xu Y, Zangvil A, Kerberb A. SiC nanoparticle-reinforced Al_2O_3 matrix composites: role of intra- and intergranular particles. *J Eur Ceram Soc* 1997;**17**:92l–8.
12. Zhang FC, Wang TS, Luo HH, Roberts SG, Todd RI. Influence factors on wear resistance of two alumina matrix composites. *Wear* 2008;**265**: 27–33.
13. Zhang FC, Luo HH, Roberts SG. Mechanical properties and microstructure of Al2O3/mullite composite. *J Mater Sci* 2007;**42**:6798–802.
14. Mezquita S, Moreno R, Baudín C. Influence of mullite additions on thermal shock resistance of dense alumina materials. Part I. Processing studies. *Brit Ceram Trans* 2001;**100**(6):241–5.
15. Burgos-Montes O, Moreno R. Colloidal behaviour of mullite powders produced by combustion synthesis. *J Eur Ceram Soc* 2007;**27**:4751–7.
16. Abercrombie M. Estimation of nuclear population from microtome sections. *Anat Rec* 1946;**94**:239–47.
17. Green DJ. *An Introduction to the Mechanical Properties of Ceramics*. Cambridge: Cambridge University Press; 1998.
18. Kreher W, Pompe W. *Internal Stresses in Heterogeneous Solids*. Berlin: Akademie Verlag; 1988.
19. Munro RG. Material properties of a sintered alpha-SiC. *J Phys Chem Ref Data* 1997;**26**:1195–203.
20. Tarlazzi A, Roncari E, Pinasco P, Guicciardi S, Melandri C, De Portu G. Tribological behaviour of Al_2O_3/ZrO_2–ZrO_2 laminated composites. *Wear* 2000;**244**:29–40.
21. Niihara K. New design concept of structural ceramics. Ceramic nanocomposites. *J Ceram Soc Jpn* 1991;**99**(10):974–82.
22. Borsa CE, Jiao S, Todd RI, Brook RJ. Processing and properties of Al_2O_3/SiC nanocomposites. *J Microsc* 1995;**177**(3):305–12.
23. Jiao S, Jenkins L, Davidge RW. Interfacial fracture energy–mechanical behaviour relationship in Al_2O_3/SiC and Al_2O_3/TiN nanocomposites. *Acta Mater* 1997;**45**(1):149–56.